Structure of the neutron-halo nucleus ^{6}He

J. Jänecke,[1] T. Annakkage,[1,*] G. P. A. Berg,[2] B. A. Brown,[3] J. A. Brown,[3] G. Crawley,[3] S. Danczyk,[3,†] M. Fujiwara,[4] D. J. Mercer,[3,‡] K. Pham,[1] D. A. Roberts,[1] J. Stasko,[3,§] J. S. Winfield,[3,‖] and G. H. Yoo[3,¶]

[1]*Department of Physics, University of Michigan, Ann Arbor, Michigan 48109-1120*

[2]*Indiana University Cyclotron Facility, Bloomington, Indiana 47408*

[3] *National Superconducting Cyclotron Laboratory, Michigan State University, East Lansing, Michigan 48824*

[4]*Research Center for Nuclear Physics, Osaka University, Osaka 567, Japan*

(Received 22 January 1996)

The ^{6}Li(^{7}Li,^{7}Be)^{6}He charge-exchange reaction leading to the neutron-halo nucleus ^{6}He has been studied at $E(^7\mathrm{Li}) = 350$ MeV. Magnetic analysis was used to observe transitions to the known $J^\pi = 0^+$ ground state and the $J^\pi = 2^+$ state at $E_x = 1.8$ MeV as well as pronounced resonances at ~5.6 MeV, ~14.6 MeV, and ~23.3 MeV. Coincidences with 430-keV Doppler-shifted γ rays from the deexcitation in flight of the $J^\pi = 1/2^-$ first-excited state in ^{7}Be were measured to permit the identification of spin-flip transitions. All observed transitions appear to have spin-flip characteristics. The shapes of the experimental angular distributions from $\theta_{\mathrm{c.m.}} = 0°$ to 18° are well described by microscopic one-step finite-range distorted-wave calculations with theoretical shell-model transition amplitudes. For the two low-lying shell-model states the absolute cross sections are also well described. The internal structures of the projectile and ejectile are taken into consideration. A large number of contributions is permitted by the angular momentum couplings. Only the ground state of ^{6}He carries significant Gamow-Teller strength B(GT). Contributions with higher L values from the central spin flip and the tensor interactions $V_{\sigma\tau}$ and $V_{T\tau}$ are responsible for the mostly structureless distributions observed, and the 0° cross sections are not proportional to B(GT). The strong resonances at ~5.6 MeV and ~14.6 MeV are interpreted as 2^+ and $(1,2)^-$ resonances, respectively, with cross sections stronger than predicted presumably due to mixing with continuum states leading to quadrupole and dipole enhancements. It appears that the resonance at ~5.6 MeV does not represent a soft dipole mode originally predicted at E_x=4–7 MeV. [S0556-2813(96)03009-9]

PACS number(s): 24.30.Cz, 25.70.Kk, 27.20.+n

I. INTRODUCTION

Neutron-halo nuclei, including ^{6}He, have attracted considerable attention in recent years [1–7]. The halo of neutrons manifests itself in several effects, including large matter radii, resulting in increased total absorption cross sections, special characteristics of the momentum distribution observed in breakup reactions, and the possible presence of ''soft giant dipole'' resonances at low excitation energies. One might expect that the energy level scheme for ^{6}He should reflect upon the halo structure. The known level scheme [8] appears to be incomplete and to contain inconsistencies. The $J^\pi = 0^+$ ground state and the first-excited $J^\pi = 2^+$ state at $E_x = 1.797$ MeV are confirmed in numerous reactions [8]. The predicted dominance of the Gamow-Teller strength B(GT) for the transition to the ground state of ^{6}He (see Sec. IV) is confirmed by the strong ground-state transition seen in (n,p) spectra [9,10] at $\theta = 0°$ and bombarding energies $\geqslant$200 MeV. However, (n,p) spectra measured at a lower bombarding energy of 60 MeV [11] and summed over the angular range from 6.5° to 32.5° display additional broad structures at $E_x = 15.5$ MeV ($\Gamma = 4$ MeV) and $E_x = 25$ MeV ($\Gamma = 8$ MeV). The radiative pion capture reaction ^{6}Li(π^-,γ)^{6}He selectively excites simple one-particle–one-hole ($1p$–$1h$) states involving spin flip; hence, $\Delta S = 1$, $\Delta T = 1$, with $L = 0$ or $L = 1$, and states at $E_x = 0.0$, 1.8, 15.6, and 23.2 MeV were observed [12,13] in agreement with the (n,p) data. However, inconsistencies are also reported [8] including the possible splitting of the 15.6-MeV resonance into two or three components over the range E_x = 13–18 MeV, observed in ^{7}Li(p,2p)^{6}He [14], ^{7}Li(n,d)^{6}He [15], ^{6}Li(e^-,π^+)^{6}He, and ^{6}Li(γ,π^+)^{6}He [16]. The latter two reactions selectively excite spin dipole resonances. Additional structures were reported [8] at $E_x = 29.7$ MeV, 32.0 MeV, and 35.7 MeV but not confirmed by other reactions. The reported levels for $E_x \leqslant 25$ MeV are included in Table I.

Soft giant dipole resonances at low excitation energies have been suggested and predicted theoretically [1,3] as a consequence of the neutron-halo structure. A resonancelike structure at $E_x \approx 6$ MeV in ^{6}He with $\Gamma \approx 4.8$ MeV has been reported [17] in the ^{6}Li(^{7}Li,^{7}Be)^{6}He reaction at $E(^7\mathrm{Li}) = 82$ MeV $= 12$A MeV. Data measured at a few angles were taken as being compatible with the assignment $L = 1$. However, recent calculations [4,5,18–20] to describe the binding

*Present address: Grafton, Auckland 1001, New Zealand.

†Present address: Department of Mechanical Engineering, Texas A&M University, College Station, TX 77843.

‡Present address: Department of Physics, University of Colorado, Boulder, CO 80309.

§Present address: Ford Research Laboratory, MD3429, 2000 Rotunda Drive, Dearborn, MI, 48121.

‖Present address: Ganil, B. P. 5027, 14021 Caen Cedex, France.

¶Present address: Department of Physics, Dae Bull Institute of Science and Technology, Seoul, South Korea.

TABLE I. Experimental excitation energies E_x, widths Γ, spin parities J^π, center-of-mass cross sections at $\theta_{\text{c.m.}} \approx 4.5°$ ($\theta_{\text{lab}} = 2°$), and averaged spin-flip signatures $G = Y_{\text{coinc}}/Y_{\text{sngl}}$.

E_x (MeV) Expt.[a]	Γ (MeV) Expt.[a]	J^π Expt.[a]	$d\sigma/d\Omega$ (mb/sr) Expt.[a]	G Expt.[a]	E_x (MeV) Expt.[b]	Γ (MeV) Expt.[b]	J^π Expt.[b]
g.s.		0^+	0.72 ± 0.08	0.46 ± 0.05	g.s.		0^+
1.92 ± 0.17		2^+	0.25 ± 0.04	0.40 ± 0.10	1.797 ± 0.025		$(2)^+$
5.6 ± 0.3	12.1 ± 1.1	2^+	4.56 ± 0.48	0.39 ± 0.04			
14.6 ± 0.7	7.4 ± 1.0	$(1,2)^-$	2.11 ± 0.23	0.43 ± 0.06	(13.6 ± 0.5)	broad	$(1^-, 2^-)$
					(15.5 ± 0.5)	4 ± 2	
23.3 ± 1.0	14.8 ± 2.3		1.75 ± 0.19	0.47 ± 0.07	(25 ± 1)	8 ± 2	

[a]Present work.
[b]Reference [8].

mechanism and excitations in the neutron-rich nucleus ^{6}He appear not to confirm the existence of a 1^- resonance in ^{6}He compatible with a soft giant dipole excitation at low excitation energy. A complex scaling method combined with a parameter-free microscopic three-cluster model was used in one theoretical approach [4,5]. Exact three-body wave functions which describe the asymptotic behavior were used to predict ground and scattering states and the strength of monopole and dipole excitations [18]. A combination of the cluster orbital shell model [21] with the extended cluster model [22] was used in another approach [19,20].

Heavy-ion-induced charge-exchange (HICEX) reactions have advantages and disadvantages as spin-isospin probes compared to high-energy (p,n) and (n,p) reactions. The energy resolution is usually better. This is particularly apparent for the (^{3}He,t) and (t,^{3}He) reactions which have characteristics much closer to (p,n) and (n,p) than more typical HICEX reactions. Certain reactions, such as (^{6}Li,^{6}He) or (^{12}C,^{12}N), are selective and, unlike (p,n) and (n,p), allow only $\Delta S = \Delta T = 1$. However, the presence of bound excited states in the ejectile may complicate the energy spectra. Complexities of HICEX reactions include (a) the possible presence of two-step contributions, (b) the presence of contributions from the tensor force resulting in strong $L = 2$ components, (c) the need to account for the internal structure of projectile and ejectile, and (d) the need to understand the strong absorption of projectile and ejectile leading to surface-dominated reactions. Many of these aspects are understood [23–25]. The (^{12}C,^{12}N) reaction at $E = 70A$ MeV [23] was found to display proportionality between $\sigma(q \approx 0)$ and B(GT) for known strong Gamow-Teller transitions. Here, q is the momentum transfer. Despite the surface character of the reaction, the contributions to the cross section from $L = 0$ are still determined by the low-momentum components of the transition densities to which the reaction is sensitive [24].

The (^{7}Li,^{7}Be) reaction was studied in the present work. This reaction presents an important tool for studying (n,p)-type charge exchange (e.g., Refs. [26–29]). The reaction was reported to proceed with a one-step reaction mechanism for energies $E \geq 21A$ MeV [28]. The nucleus ^{7}Be has two particle-stable states, the $J^\pi = 3/2^-$ ground state, $^7\text{Be}_{\text{g.s.}}$, and the $J^\pi = 1/2^-$ state at $E_x = 0.430$ MeV, $^7\text{Be}_{\text{exc}}$. Assuming a dominance of pure Fermi and/or Gamow-Teller transitions, the population of the $^7\text{Be}_{\text{g.s.}}$ proceeds by a mixture of $\Delta S = 0$ and $\Delta S = 1$, whereas that of the $^7\text{Be}_{\text{exc}}$ will proceed only with $\Delta S = 1$. It has been shown by Nakayama *et al.* [29] that by measuring coincidences with 430-keV Doppler-shifted γ rays, and thus isolating the transition to the excited $^7\text{Be}_{\text{exc}}$ state, it becomes possible to separate the $\Delta S = 0$ and $\Delta S = 1$ contributions. Using measured $\log(ft)$ values compiled in Ref. [30] to determine the Gamow-Teller strengths B(GT), one obtains

$$\sigma(^7\text{Be}_{\text{g.s.}}) = \sigma(\Delta S = 0) + 1.300\sigma(\Delta S = 1), \tag{1}$$

$$\sigma(^7\text{Be}_{\text{exc}}) = 1.124\sigma(\Delta S = 1). \tag{2}$$

This means that the ratio G defined by

$$G \equiv \frac{\sigma(^7\text{Be}_{\text{exc}})}{\sigma(^7\text{Be}_{\text{g.s.}}) + \sigma(^7\text{Be}_{\text{exc}})} \tag{3}$$

becomes equal to the ratio for the efficiency-corrected yield for ^{7}Be-γ coincidences [proportional to $\sigma(^7\text{Be}_{\text{exc}})$] and the yield for ^{7}Be singles events [proportional to $\sigma(^7\text{Be}_{\text{g.s.}}) + \sigma(^7\text{Be}_{\text{exc}})$]. According to Eqs. (1) and (2), the ratio G should therefore be equal to

$$G = \frac{Y_{\text{coinc}}}{Y_{\text{sngl}}} = 0 \quad \text{for} \quad \Delta S = 0 \ \text{transitions}, \tag{4}$$

$$G = \frac{Y_{\text{coinc}}}{Y_{\text{sngl}}} = 0.46 \quad \text{for} \quad \Delta S = 1 \ \text{transitions}. \tag{5}$$

Assignments of $\Delta S = 0$ and $\Delta S = 1$ could therefore be based on measured cross section ratios for $\theta = 0°$. However, there are experimental limitations, and the technique may be confined to light target nuclei [31] because of interference with γ rays from the deexcitation of the residual nuclei. While the Doppler shift could in principle provide a signature for the 430-keV γ rays, the usually large number of γ rays in heavier targets and the finite energy resolution may exclude this. Also, the sensitivity of many γ-ray detectors to neutrons [32,31] presents a difficulty. Furthermore, Eqs. (1) and (2) represent approximations because they ignore the tensor interaction. They also disregard the influence of the internal structures of the projectile and ejectile, which leads to often

large numbers of possible angular momentum couplings and may limit the applicability of the equations.

II. EXPERIMENTAL PROCEDURES

The experiment was carried out at the National Superconducting Cyclotron Laboratory (NSCL) with a beam of ^{7}Li projectiles of energy $E(^{7}\mathrm{Li}) = 350$ MeV $= 50A$ MeV from the K1200 superconducting cyclotron. The ^{7}Be ejectiles were detected at laboratory angles from $\theta_{\mathrm{lab}} = 2°$ to 8.5° in the focal plane of the S320 magnetic analyzer with moderate overall energy resolution of $\Delta E \approx 1.5$ MeV or $\Delta E/E \approx 4.3\times10^{-3}$. This includes the contributions from the unresolved states in ^{7}Be. Measurements at $\theta_{\mathrm{lab}} = 0°$ were performed with the A1200 magnetic analysis system with similar energy resolution. Data were obtained with the S320 spectrometer up to $E_x \approx$ 50 MeV with solid angles of $\Delta\Omega \approx$ 0.20 and 0.67 msr, and with the A1200 system up to $E_x \approx$ 20 MeV with $\Delta\Omega \approx$ 1.2 msr. Details of the experimental procedures will be reported elsewhere [31].

The charge integration for the finite-angle points was straightforward. However, the absolute calibration of the integrator for the 0° measurements caused problems because of imperfect collection efficiency. This resulted in an increased uncertainty. All relative yields for the 0° measurements for ^{6}Li and the other targets are reliable, though. Rolled enriched ^{6}Li targets of thickness $\rho\Delta x = 2.0$–2.6 mg/cm^2 were used, and care was taken to keep the targets as hydrogen free as possible. However, hydrogen contaminants were present in all targets, typically ~ 8 μg/cm^2 for ^{6}Li, exceeded only by the $^{\mathrm{nat}}$C target. Measurements with good statistics were therefore also performed with a polystyrene $(C_8H_8)_n$ target ($\rho\Delta x \approx$ 1.0–2.3 mg/cm^2) to permit the subtraction of the hydrogen contributions in all spectra.

An array of 12 bismuth germanate $Bi_4Ge_{13}O_{12}$ (BGO) scintillation detectors [33] at a distance of 6.4 cm from the target in a circular arrangement was used to record coincidences with 430-keV Doppler-shifted γ rays from the deexcitation in flight of excited $^{7}\mathrm{Be}_{\mathrm{exc}}$. Each detector covered an angular range of $\sim$15°. Using several calibrated γ-ray sources at the target position, the overall photopeak detection efficiency for 430-keV γ rays was determined to be $\sim$11%. The photofraction is $\sim$60%, and pronounced photopeaks were observed for ^{6}Li and other light targets with an energy resolution of full width at half maximum (FWHM) $\approx$ 25%. Coincidence spectra for ^{7}Be gated on true γ-ray photopeak events were obtained by subtracting in the γ-ray time-of-flight spectrum the random events from the prompt events (prompt to random ratio $\sim$20). BGO detectors are also sensitive to neutrons [32] primarily due to the detection of γ rays from inelastic scattering of neutrons in the scintillator material. A weak background in the BGO pulse-height spectra above the photopeak was observed due to the sensitivity to neutrons. These contributions were subtracted by assuming a linear extrapolation to lower pulse heights. The corrected coincidence yield observed for established Gamow-Teller transitions confirmed the above γ-ray detection efficiency of $\sim$11%.

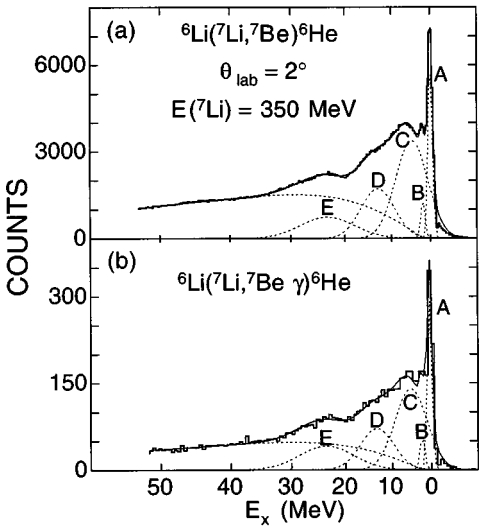

FIG. 1. Spectra of ^{7}Be ejectiles from the reaction ^{6}Li(^{7}Li, ^{7}Be)^{6}He measured at $\theta_{\mathrm{lab}} = 2°$ in singles mode (a), and in coincidence with 430-keV γ rays from $^{7}\mathrm{Be}_{\mathrm{exc}} \rightarrow {}^{7}\mathrm{Be}_{\mathrm{g.s.}} + \gamma$ (b). *A*, g.s.; *B*, 1.8 MeV; *C*, 5.6 MeV; *D*, 14.6 MeV; *E*, 23.3 MeV. The dotted lines represent the decomposition into resonances and nonresonant background (see text).

III. EXPERIMENTAL RESULTS

Spectra measured at $\theta_{\mathrm{lab}} = 2°$ in singles mode and in coincidence mode are shown in Fig. 1. Contributions from hydrogen near the ground state were removed by subtracting independently measured and properly normalized spectra obtained with a polystyrene target. These contributions become kinematically defocused with increasing reaction angle, and the region of interference is strongest at $\theta_{\mathrm{c.m.}} \approx 5°$ for the ground state and at $\theta_{\mathrm{c.m.}} \approx 14°$ for the state at 23.3 MeV. The spectra in Fig. 1 display the transitions to the states at $E_x =$ 0.0 and 1.8 MeV, as well as strong and broad resonances at $\sim$5.6, $\sim$14.6, and $\sim$23.3 MeV excitation energy. Cross sections $d\sigma/d\Omega$, excitation energies E_x, and widths Γ were extracted for all measured spectra.

A nonresonant background from quasifree charge exchange on bound protons, $p_{\mathrm{bound}}(^{7}\mathrm{Li},^{7}\mathrm{Be})n_{\mathrm{free}}$, [34–37] was included in the fitting procedure. The removal of a neutron leaves the residual nucleus usually in its ground state. The Fermi motion of the bound proton in the target nucleus leads to a Lorentzian line shape with an energy broadening characterized by the energy term W in the equation

$$\frac{d^2\sigma}{dEd\Omega} = N_0 \frac{1-\exp[(E_{^{7}\mathrm{Be}}-E_0)/T]}{1+[(E_{^{7}\mathrm{Be}}-E_{\mathrm{QF}})/W]^2}. \tag{6}$$

The centroid energy E_{QF} of the quasifree process is shifted relative to that of the charge-exchange process on a free proton by the neutron binding energy in ^{6}He of $S_n = 1.869$ MeV. Unlike (p,n)-type reactions [34–37] no shift due to a Coulomb barrier needs to be included; hence, $E_{\mathrm{QF}} = E_{^{7}\mathrm{Be}}(\mathrm{free}) - \mathrm{S_n}$. This energy depends strongly on the reaction angle. In addition, an exponential term due to Pauli blocking is included. Here, the quantity T has the characteristics of a temperature, and the cutoff energy E_0

represents the threshold for three-body breakup, $E_0 = E_{^7\mathrm{Be}}(^6\mathrm{He}_{\mathrm{g.s.}}) - S_n$. This energy depends weakly on the reaction angle.

The energies E_{QF} and E_0 were set at their calculated values, and the two additional parameters were fixed at $W = 32$ MeV and $T = 90$ MeV. The latter value agrees with values determined earlier for pion and (^{3}He,t) charge-exchange experiments [34–37], whereas $W = 32$ MeV is larger than $W \approx 22$ MeV which was usually found to give best agreement. Larger values of $W \approx 28$ MeV and 35 MeV, however, are also reported [35]. Even though the calculated shapes are not very sensitive to the choice of parameters [36], an independent search was performed which favored the larger value mostly on the basis of the data at high excitation energies as can be seen from Fig. 1.

The amplitudes N_0 together with the quantities describing the observed resonances were used as adjustable parameters for all singles and coincidence spectra. Equation (6) describes the observed spectral shapes for the regions above the highest observed resonance rather well at all angles. The comparison with the data becomes more difficult only at the largest angles because E_{QF} changes significantly with increasing angle, shifting the maximum of the distribution towards $E_x \approx 50$ MeV.

It is interesting to note that Eq. (6) seems to describe quite well the nonresonant background from quasifree charge exchange for several rather different (p,n)-type and (n,p)-type reactions.

Energy-integrated cross sections for the nonresonant background of the simultaneously measured singles and coincidence spectra (see, e.g., Fig. 1) made it possible to determine consistent cross section ratios of $G \approx 29.3\%$. This suggests a mixture of non-spin-flip and spin-flip transitions with a weak enhancement of non spin flip. Nakayama *et al.* [29] have similarly found an approximately equal mixture of non-spin-flip and spin-flip contributions to the continuum up to an excitation energy of 18 MeV for ^{12}C(^{7}Li,^{7}Be)^{12}B at a bombarding energy of $E(^7\mathrm{Li}) = 26A$ MeV.

Angular distributions with the small aperture of $\Delta\Omega \approx 0.20$ msr and hence good angle definition of $\pm 0.3°$ were measured in singles mode over the entire angular range in steps of 0.5° without resolving the transitions to $^7\mathrm{Be}_{\mathrm{g.s.}}$ and $^7\mathrm{Be}_{\mathrm{exc}}$. The results for the five transitions are displayed in Fig. 2 and are included in Table I for $\theta_{\mathrm{lab}} = 2°$.

The estimated uncertainties reflect upon the uncertainties of the peak fitting procedures including the subtraction of the nonresonant background, the charge integration, particularly for the data points at $\theta \approx 0°$, corrections for the hydrogen subtraction, and to a lesser extent the statistics of the data. The absolute uncertainties are estimated at $\pm 20\%$ mostly from the uncertainty of the target thickness and possible global effects from background subtraction. A systematic reduction by 20–30 % in the cross sections for the resonances at $\sim$14.6 MeV and $\sim$23.3 MeV is possible if the Fermi-energy parameter W in Eq. (6) had to be reduced to $W \approx 22$ MeV, whereas excitation energies and widths are not affected.

All cross sections decrease with increasing angle and the distributions are rather structureless. However, the slopes are different, and the transitions to the resonance at 23.3 MeV show an almost constant cross section. Only the transition to the ground state displays a strong increase towards $\theta = 0°$.

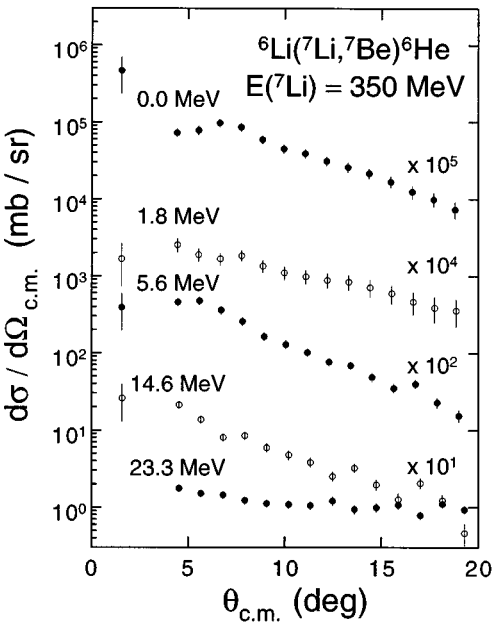

FIG. 2. Experimental angular distributions for the transitions to the states at $E_x = 0.0$ MeV, 1.8 MeV, 5.6 MeV, 14.6 MeV, and 23.3 MeV obtained in singles mode without the separation into the $^7\mathrm{Be}_{\mathrm{g.s.}}$ and $^7\mathrm{Be}_{\mathrm{exc}}$ components.

The excitation energies E_x and widths Γ are included in Table I together with the known energies from Ref. [8]. They were obtained by averaging the results from all singles and coincidence data.

Coincidence measurements were performed with a larger aperture of $\Delta\Omega \approx 0.67$ msr for only a few selected angles of $\theta_{\mathrm{lab}} = 0°$, 2°, 3°, 4°, 5°, and 6°. Clean photopeaks for the 430-keV Doppler-shifted γ rays were observed.

Using the detection efficiency for the γ rays obtained from γ-ray calibration sources, cross section ratios $G = Y_{\mathrm{coinc}}/Y_{\mathrm{sngl}}$ defined in Eq. (3) were extracted for all angles. The averaged values are included in Table I for comparison with Eqs. (4) and (5). Any systematic errors are reduced because singles and coincidence spectra are measured simultanously.

Whereas the above ratios G are quite reliable, the extraction of complete spectra for $\sigma(\Delta S = 0)$ and $\sigma(\Delta S = 1)$ defined in equations Eqs. (1) and (2) is in principle possible for all angles. In fact, the $\sigma(\Delta S = 1)$ are equal to the measured coincidence spectra corrected for the γ-ray detection efficiency and the factor in Eq. (2). However, it was found that $\sigma(\Delta S = 0)$ cannot be reliably extracted due to limited statistics and the fact (see Sec. V E) that all transitions appear to have spin-flip characteristics.

IV. DISTORTED-WAVE ANALYSIS

A. Transition amplitudes

Microscopic distorted-wave Born approximation (DWBA) calculations were performed. The calculations of the transition densities requires knowledge of the wave functions for the projectile and the ejectile as well as the target nucleus and the final states in the residual nucleus. Cohen-Kurath wave functions were used [38] for all states except

TABLE II. Calculated Gamow-Teller strengths B(GT) for the two particle-stable states in ^{7}Be.

E_x (MeV) Expt.[a]	J^π Expt.[a]	B(GT) Expt.[b]	B(GT) WS Calc.[c]	Ratio
g.s.	$3/2^-$	1.2999 ± 0.0036	1.6215	0.802
0.429	$1/2^-$	1.1236 ± 0.0067	1.3305	0.845

[a]Reference [8].
[b]Reference [29].
[c]Present work.

the positive-parity states in ^{6}He which are described below. The wave functions were constructed with Woods-Saxon radial shapes and experimental separation energies. Tables II and III include the experimental and calculated Gamow-Teller strengths B(GT) for the $A=7$ and $A=6$ systems, respectively. The experimental values are based on the measured log(ft) values compiled in Ref. [30]. The value for $^7\mathrm{Be}_{\mathrm{exc}}$ is taken from the β decay of the mirror system $^7\mathrm{Be}_{\mathrm{g.s.}} \rightarrow {}^7\mathrm{Li}_{\mathrm{exc}}$. The calculated B(GT) values make use of transition densities obtained with Woods-Saxon wave functions for the ^{7}Li-^{7}Be and ^{6}Li-^{6}He systems; for the ^{6}Li-^{6}He system almost identical values, differing by only 3%, were also obtained with harmonic oscillator wave functions. The calculated B(GT) values deviate from the experimental values by $<20\%$. This agrees well with deviations between calculated and experimental B(GT) values reported previously (see Table II in Ref. [23]). All calculated angular distributions (see below) were corrected by the ratios of the experimental to calculated B(GT) for the transitions to $^7\mathrm{Be}_{\mathrm{g.s.}}$ and $^7\mathrm{Be}_{\mathrm{exc}}$, respectively.

The wave functions for the positive-parity states in ^{6}He were obtained using the approach reported earlier [39] for the prediction of the binding energy of ^{10}He. Shell-model Hamiltonians in the $0p$ model space which are optimized to fit the binding energies and excitation energies of all $0p$ shell nuclei from $A=5$ to $A=16$ do particularly poorly for ^{6}He. With the earliest [38] as well as with the more recent [40] full $0p$-shell interactions, the 2^+ excitation energy in ^{6}He is predicted at ~ 4 MeV compared to its experimental value of 1.80 MeV and the experimental energy difference of the $T=1$ analog states in ^{6}Li of 1.81 MeV. This is presumably related to the halo nature of the two valence neutrons in ^{6}He. To take this into account, another effective interaction for the He isotopes was developed in which the Hamiltonian parameters were obtained from the binding energies of eight known states in the He isotopes [39]. These data were successfully fit by adjusting the strengths of three central $T=1$ two-body interaction parameters and two single-particle energies and leaving the less important spin-orbit and tensor parts of the $T=1$ two-body interaction at their G matrix values. The original goal of this He interaction was to predict the masses and excitation energies of unknown states [39]. In particular, ^{10}He was predicted to be unbound relative to ^{8}He, and recent reaction measurements for the ^{10}He mass are in good agreement with this prediction [41]. Thus, we use a Hamiltonian which combines the $T=0$ part of the traditional (6-16) two-body matrix elements from the interaction of Cohen and Kurath [38] with this improved $T=1$ interaction from [39]. The calculated excitation energies are included in Table III together with the respective B(GT) values.

The transition amplitudes for the present calculations were calculated with transition densities generated by the shell-model code OXBASH [42]. They are based on the $0p$-shell-model space (CKHE, CKI) or, for the negative parity states in ^{6}He, on the $0s0p1s0d$-shell-model space (SPSDMK). The latter space allows excitations from the $0s_{1/2}$ shell into the p shell and from the p shell into the ds shell. Special effective interactions are used for the positive-parity states in ^{6}He (CKHE), as described above, whereas the traditional (6-16) two-body matrix elements from the interaction of Cohen and Kurath [38] (CKI) are used for ^{6}Li, ^{7}Li, and ^{7}Be. The interactions of Millener and Kurath [43,44] (SPSDMK) are used for the negative-parity states in ^{6}He.

Independent calculations for states in ^{6}He have been performed recently by Csótó [4,5], by Danilin *et al.* [18], and by Aoyama *et al.* [19,20]. However, transition amplitudes are not reported. The calculations by Csótó [4,5] make use of a complex scaling method in a parameter-free three-cluster model to calculate low-lying resonances in ^{6}He, ^{6}Li, and ^{6}Be and the two-neutron separation energy of ^{6}He. Clusterizations $\alpha+n+n$ and $t+t$ and α-cluster breathing excita-

TABLE III. Experimental and calculated excitation energies E_x, widths Γ, and Gamow-Teller strength B(GT) for positive-parity states in ^{6}He (see text).

E_x (MeV) Expt.[a]	E_x (MeV) Calc.[a]	E_x (MeV) Calc.[b]	J^π Calc.[a,b]	Γ (MeV) Expt.[a]	Γ (MeV) Calc.[b]	B(GT) Expt.[c]	B(GT) HO Calc.[a]	B(GT) WS Calc.[a]	Ratio
g.s.	g.s.	g.s.	0^+			1.576 ± 0.005	1.843	1.783	0.855
1.797 ± 0.025[d]	1.894	1.81	2^+		0.26		0.006	0.006	
5.6 ± 0.6	6.124	3.40	2^+	10.9 ± 1.9	4.21		0.190	0.184	
	7.268	3.75	1^+		6.39		0.103	0.100	
	12.467	4.99	0^+		8.87		0.064	0.063	

[a]Present work.
[b]References [18],[19].
[c]Reference [29].
[d]Reference [8].

TABLE IV. Combinations of angular momentum values J_p, J_t, and L with $\vec{L} = \vec{J_p} + \vec{J_t}$ for ^{6}Li(^{7}Li,^{7}Be)^{6}He with $J^\pi(^7\text{Li}) = 3/2^-$, $J^\pi(^7\text{Be}_{\text{g.s.}}) = 3/2^-$, $J^\pi(^7\text{Be}_{\text{exc}}) = 1/2^-$, $J^\pi(^6\text{Li}) = 1^+$, and $J^\pi(^6\text{He}) = 0^+$, 1^-, or 2^+.

$1^+ \rightarrow 0^+$	^{7}Be$_{\text{g.s.}}$													^{7}Be$_{\text{exc}}$						
J_p		0			1			2			3				1			2		
J_t		1			1			1			1				1			1		
L					0										0					
					2			2			2				2			2		
											4									
$1^+ \rightarrow 1^-$																				
J_p		0	0	0	1	1	1	2	2	2	3	3	3		1	1	1	2	2	2
J_t		0	1	2	0	1	2	0	1	2	0	1	2		0	1	2	0	1	2
L			1		1	1	1		1	1			1		1	1	1		1	1
							3		3	3	3	3	3				3		3	3
													5							
$1^+ \rightarrow 2^+$																				
J_p		0	0	0	1	1	1	2	2	2	3	3	3		1	1	1	2	2	2
J_t		1	2	3	1	2	3	1	2	3	1	2	3		1	2	3	1	2	3
L					0				0				0		0				0	
			2		2	2	2	2	2	2	2	2	2		2	2	2	2	2	2
							4		4	4	4	4	4				4		4	4
													6							

tions were included to establish the neutron halo of ^{6}He. The originally predicted [3] soft dipole mode could not be confirmed.

The calculations by Danilin *et al.* [18] employ exact three-body wave functions expanded in hyperspherical harmonics which describe the asymptotic behavior of boromean systems. The authors calculated strength functions of electric dipole and nuclear monopole excitations, and they observed a considerable concentration of strength at lower energies, but no narrow resonances.

The calculations of Aoyama *et al.* [19,20] make use of the cluster orbital shell model [21] in combination with the extended cluster model [22]. This ''hybrid-*TV*'' model was used to calculate the binding energy of the ground state of ^{6}He and the excitation energies E_x of positive-parity states. These values are included in Table III. While only the basic *p*-shell components of these states are reported, continuum state admixtures permitted the calculation of widths Γ for these states. The authors do also not confirm the possible presence of a soft giant dipole resonance at low excitation energy.

B. Calculation of angular distributions

One-step DWBA calculations were carried out with the reaction code FOLD developed by Cook and Carr [45] based on the code originally used by Petrovich and Stanley [46] and modified as reported by Cook *et al.* [27]. The code was previously used by Anantaraman *et al.* [23] for the (^{12}C, ^{12}N) reaction at $E = 70A$ MeV describing transitions from the $J^\pi = 0^+$ target to 1^+ final states. The formalism includes the direct central terms including exchange and direct tensor terms (see Ref. [23]).

Since the projectile and ejectile have internal structures, appropriate angular momentum labels have to be introduced. The total angular momentum transfer in the relative coordinates is $\vec{J_r} = \vec{J_p} + \vec{J_t}$. If only central and tensor forces are considered, $\vec{J_r} = \vec{L}$, where L is the orbital angular momentum transfer. Here, $\vec{J_p}$ and $\vec{J_t}$ are the total angular momenta transferred to the projectile and the target, respectively. Furthermore, since $\vec{J_p} = \vec{L_p} + \vec{S_p}$ and $\vec{J_t} = \vec{L_t} + \vec{S_t}$, even a simple $J_p = 1$ without change in parity permits $S_p = 1$ with $L_p = 0$ *and* $L_p = 2$.

The (^{7}Li,^{7}Be) reaction on a ^{6}Li target allows many components because J_p can take on the values $J_p = 0$, 1, 2, and 3 for transitions to ^{7}Be$_{\text{g.s.}}$ and in addition $J_p = 1$ and 2 for transitions to ^{7}Be$_{\text{exc}}$. Also, except for final states with $J^\pi = 0^+$, three values for J_t are possible. Table IV shows all possible combinations of the angular momentum labels (L, J_p, J_t) for three examples, namely, transitions to final states in ^{6}He with $J^\pi = 0^+$, 1^-, and 2^+. The orbital angular momenta L are subject to parity conservation. For transitions to $J^\pi = 0^+$ states in ^{6}He there are $5 + 3 = 8$ components with $L = 0$, 2, and 4 for ^{7}Be$_{\text{g.s.}}$, namely, (0,1,1), (2,1,1), (2,2,1), (2,3,1), (4,3,1) plus (0,1,1), (2,1,1), (2,2,1) for ^{7}Be$_{\text{exc}}$. For $J^\pi = 1^-$ states in ^{6}He there are $14 + 8 = 22$ components with $L = 1$, 3, and 5. For $J^\pi = 2^+$ states in ^{6}He there are $20 + 11 = 31$ components with $L = 0$, 2, 4, and 6. The specific calculations presented below show that the relative strength of these components varies strongly in their incoherent superposition. The number of components for the (^{7}Li,^{7}Be) reaction on targets with $J^\pi = 0^+$, such as ^{12}C, is smaller because J_t can take on only a single value for any final state, as is the case for the transition from ^{6}Li to the $0+$ ground state of ^{6}He. Other HICEX reactions permit an even more limited number of components. For example, the above (^{12}C,^{12}N) work [23] for $0^+ \rightarrow 1^+$ transitions gives only two components with $J_p = 1$, $J_t = 1$, and $L = 0$ and 2, i.e., with angular momentum labels (0,1,1) and (2,1,1). Here, the contributions are from the central interaction with $L = 0$, 2

TABLE V. Optical-model parameters for ^{7}Li scattering from ^{6}Li and ^{12}C targets at $E(^7\mathrm{Li}) = 350$ MeV (see text).

	V_0 (MeV)	r_0 (fm)	a (fm)	V_{0I} (MeV)	r_{0I} (fm)	a_I (fm)	r_C (fm)
^{6}Li	-107.8	1.538	0.853	-37.9	1.870	0.757	1.342
^{12}C	-107.8	1.375	0.853	-37.9	1.672	0.757	1.200

and the tensor interaction with $L=2$.

The reaction code FOLD [45] permits the use of the effective nucleon-nucleon interactions of Love and Franey [47,48] and the modified M3Y interaction of Petrovich *et al.* [49]. Angular distributions for $^6\mathrm{Li}(^7\mathrm{Li},^7\mathrm{Be})^6\mathrm{He}_{\mathrm{g.s.}}$ and $^{12}\mathrm{C}(^7\mathrm{Li},^7\mathrm{Be})^{12}\mathrm{B}_{\mathrm{g.s.}}$ based on the 50- and 100-MeV t-matrix interactions of Love and Franey [48] and the M3Y interaction of Ref. [49] differ only little with a slight preference for M3Y which was used for all subsequent calculations.

The optical-model parameters for elastic scattering of ^{7}Li projectiles on targets of ^{12}C and ^{28}Si at $E(^7\mathrm{Li}) = 350$ MeV were obtained recently by Nadasen *et al.* [50]. The radius parameter $\tilde{r}_0$ in the heavy-ion convention $R=\tilde{r}_0(A_{\mathrm{tgt}}^{1/3}+A_{\mathrm{proj}}^{1/3})=r_0A_{\mathrm{tgt}}^{1/3}$ was found to be almost identical for the two targets. Similar results were observed earlier for ^{6}Li elastic scattering at $E(^6\mathrm{Li}) = 210$ MeV on six targets from ^{12}C to ^{208}Pb [51]. Therefore, the same radius parameter $\tilde{r}_0$ was assumed for the extrapolation of the optical-model parameters for 350-MeV elastic ^{7}Li scattering [50] from the ^{12}C target to the ^{6}Li target. The optical-model parameters for ^{7}Li used in the present work are listed in Table V. The parameters for ^{7}Be were set equal to those for ^{7}Li.

The following subsection describes the results of the calculations for the states and resonances in ^{6}He and compares the calculated distributions with the experimental distributions.

C. Predictions for ^{6}Li(^{7}Li,^{7}Be)^{6}He

Figures 3–6 display the experimental angular distributions together with calculated distributions obtained with the above transition densities, optical-model parameters, and the effective M3Y nucleon-nucleon interaction for the states in ^{6}He at $E_x = 0.0$, 1.8, 5.6, and 14.6 MeV. The complete decomposition into the components with angular momentum labels (L,J_p,J_t) is shown in Figs. 3 and 4 for the transitions to the states at $E_x = 0.0$ and 1.8 MeV. Transitions to both $^7\mathrm{Be}_{\mathrm{g.s.}}$ and $^7\mathrm{Be}_{\mathrm{exc}}$ are permitted for $J_p = 1$ or 2. Therefore, most of these components show two closely neighboring curves. They are displayed with the same label. These figures also display separately the calculated cross sections from the central and the tensor interaction, respectively, including the decomposition into all angular momentum components (L,J_p,J_t).

Figures 5 and 6 display for the resonances at $E_x \approx 5.6$ and 14.6 MeV the experimental angular distributions together with four calculated distributions each. As described in the previous section, the transition amplitudes for the assumed positive- and negative-parity states were calculated with the shell-model transition densities CKHE, CKI, and SPSDMK. Angular distributions were also calculated for the state at $E_x = 23.3$ MeV, but no satisfactory fit could be obtained for the rather flat angular distribution (see Fig. 2).

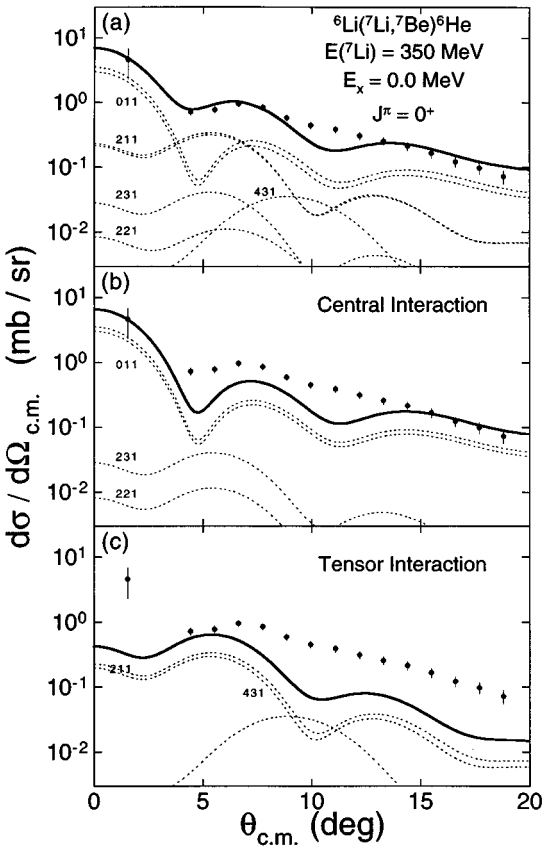

FIG. 3. Experimental and calculated angular distributions for the transition to the $J^\pi = 0^+$ ground state of ^{6}He with decomposition (see text) into all components permitted by $\vec{L} = \vec{J_p} + \vec{J_t}$ (a), and with the additional decomposition into contributions from the central (b) and tensor (c) nucleon-nucleon interactions. Assignments (L,J_p,J_t) are indicated. The normalization factors and goodness-of-fit parameters are included in Table VI.

The least-squares adjustments of the calculated angular distributions to the data points of Figs. 3–6 make use of one single adjusted parameter each, the overall normalization factor f. Table VI lists these values of f and the goodness-of-fit values per degree of freedom, χ^2/F, for all transitions characterized by the excitation energies E_x and spin parities J^π. Column 3 defines the states identified by the shell-model code OXBASH [42]. Here, J_i^π stands for the ith state in ^{6}He with spin parity J^π (with the model spaces and effective interactions CKHE for $\pi = +1$ and SPSDMK for $\pi=-1$). The agreement between the experimental and calculated distributions is quite good for the states at $E_x = 0.0$, 1.8, 5.6, and 14.6 MeV with $J^\pi = 0_1^+$, 2_1^+, 2_2^+, and 1_1^-, respectively. The goodness-of-fit values per degree of freedom, χ^2/F, range from 1.2 to 3.7.

All calculated angular distributions were decomposed into central and tensor components which is shown explicitely for $E_x = 0.0$ and 1.8 MeV in Figs. 3 and 4. Considering the possible need for a relative renormalization of the tensor interaction, several experimental distributions were also fitted by using an incoherent superposition of the central and tensor components with independent normalization factors f_C and f_T. Only minor improvements in the goodness of fit

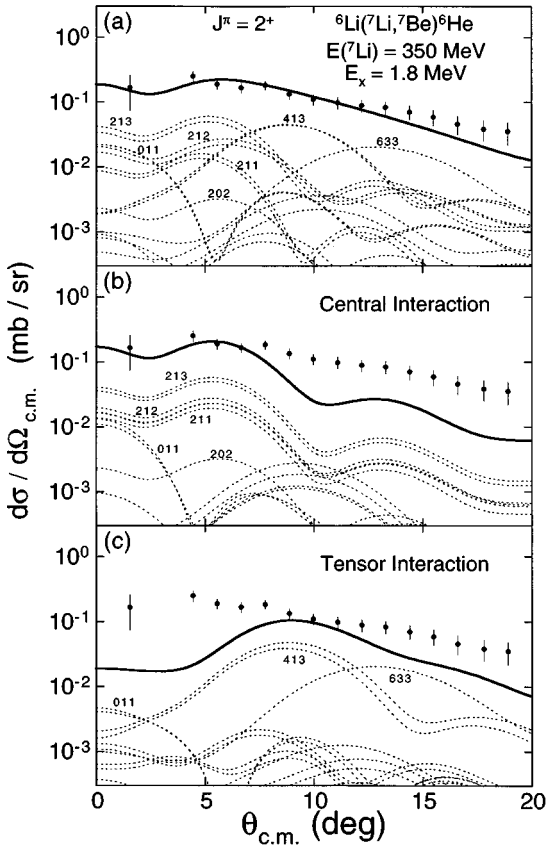

FIG. 4. Experimental and calculated angular distributions for the weak transition to the $J^\pi = 2^+$ state at 1.8 MeV of ^{6}He with decomposition (see text) into all components permitted by $\vec{L} = \vec{J_p} + \vec{J_t}$ (a), and with the additional decomposition into contributions from the central (b) and tensor (c) nucleon-nucleon interactions. Assignments (L, J_p, J_t) are indicated. The normalization factors and goodness-of-fit parameters are included in Table VI.

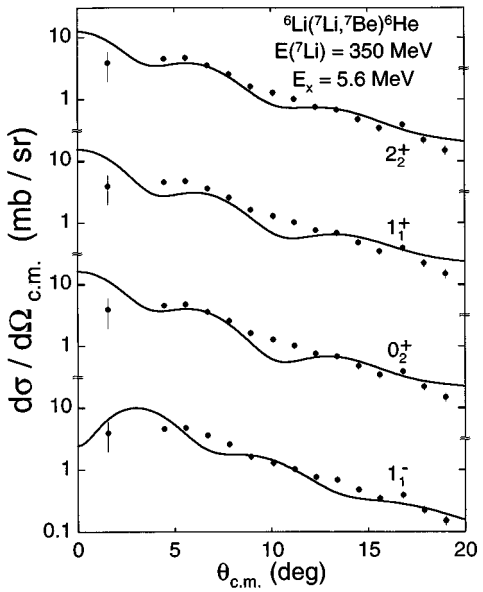

FIG. 5. Experimental and calculated angular distributions for the transition to the $J^\pi = 2^+$ state in ^{6}He at $E_x = 5.6$ MeV without decomposition into components. The four calculated transitions are for assumed shell-model states of 2_2^+, 1_1^+, 0_2^+, and 1_1^-. The normalization factors and goodness-of-fit parameters are included in Table VI.

were achieved. The ratios f_T/f_C of these factors are shown in the last column of Table VI.

D. Predicted cross section ratios $G \equiv \sigma(^7\mathrm{Be_{exc}})/[\sigma(^7\mathrm{Be_{g.s.}}) + \sigma(^7\mathrm{Be_{exc}})]$

The calculated cross section ratios G are shown in Fig. 7 as function of the angle $\theta_{\mathrm{c.m.}}$ for the transitions to the four states in ^{6}He. They were obtained by adding in Figs. 3 – 6 the cross sections for all components (denominator) and only those components resulting from transitions to $^7\mathrm{Be}_{\mathrm{exc}}$ (numerator). The ratios are not constant as function of angle but display structures, particularly at larger angles. Cross section ratios G_L were also calculated separately for each contributing value of L. These ratios G_L, also included in the figures, display a different dependence on angle. In particular, $G_L \equiv 0$ for the highest possible L values of $L = 4$, 6, 6, and 5, respectively, where only the transition to $^7\mathrm{Be}_{\mathrm{g.s.}}$ is permitted due to the tensor interaction. The weighted ratios G_L are equal to the ratios G shown in the figure.

Table VII lists the ratios G_i at $\theta = 0°$ for all permitted angular momentum labels (L, J_p, J_t). They are given for the 0^+, 2^+, 2^+, and 1^- states at $E_x = 0.0$, 1.8, 5.6, and 13.2 MeV, respectively. There are 5, 20, 20, and 14 ratios, respectively. For $J_p = 1$, the ratios are in the range $G_i = 0.45$–0.52 and therefore close to $G_i = 0.46$ as expected from Eqs. (5) for spin-flip transitions. For some labels only transitions to $^7\mathrm{Be}_{\mathrm{g.s.}}$ are permitted ($G_i \equiv 0$ for $J_p = 0$ and 3), and for some labels only transitions to $^7\mathrm{Be}_{\mathrm{exc}}$ are permitted ($G_i \approx 1$ for $J_p = 2$). Also included in the table are the weighted

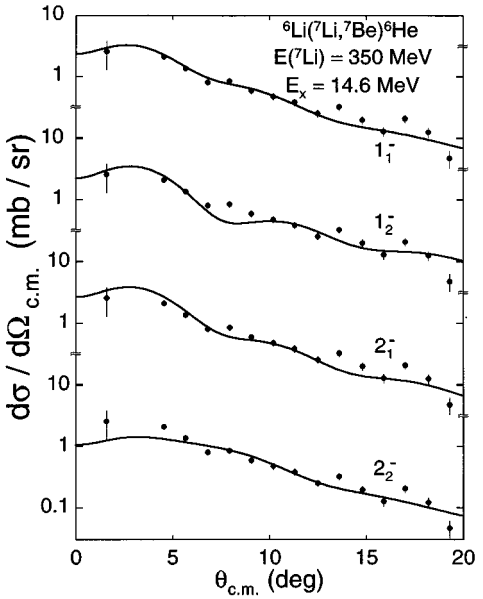

FIG. 6. Experimental and calculated angular distributions for the transition to the $J^\pi = 1^-$ state in ^{6}He at $E_x = 14.6$ MeV without decomposition into components. The four calculated transitions are for assumed shell-model states of 1_1^-, 1_2^-, 2_1^-, and 2_2^-. The normalization factors and goodness-of-fit parameters are included in Table VI.

TABLE VI. Normalization factors f and goodness of fit per degree of freedom χ^2/F for calculated angular distributions (see text).

E_x (MeV)	J^π	J_i^π	f	$f^{\rm corr}$	χ^2/F	f_T/f_C
g.s.	0^+	0_1^+	0.648	0.734	3.66	1.01
1.8	2^+	2_1^+	0.707		1.22	1.37
5.6	2^+	2_2^+	12.61		3.61	19.82
5.6	1^+	1_1^+	30.82		8.08	
5.6	0^+	0_2^+	50.94		5.98	
5.6	1^-	1_1^-	21.81		5.59	
5.6	$(2^+, 1^+)$	$2_2^+ + 1_1^+$	8.99		5.00	
14.6	1^-	1_1^-	11.38		2.42	1.10
14.6	1^-	1_2^-	13.23		4.67	
14.6	2^-	2_1^-	10.54		3.42	
14.6	2^-	2_2^-	4.98		3.22	
14.6	2^+	2_2^+	5.97		3.39	
14.6	1^+	1_1^+	17.29		4.58	
14.6	0^+	0_2^+	26.41		4.32	
23.3	1^-	1_1^-	25.38		28.65	
23.3	1^-	1_2^-	39.52		26.98	
23.3	2^-	2_1^-	24.53		32.76	
23.3	2^-	2_2^-	10.66		21.93	

averages G_L and G which are identical to the values shown in Fig. 7 at $\theta = 0°$.

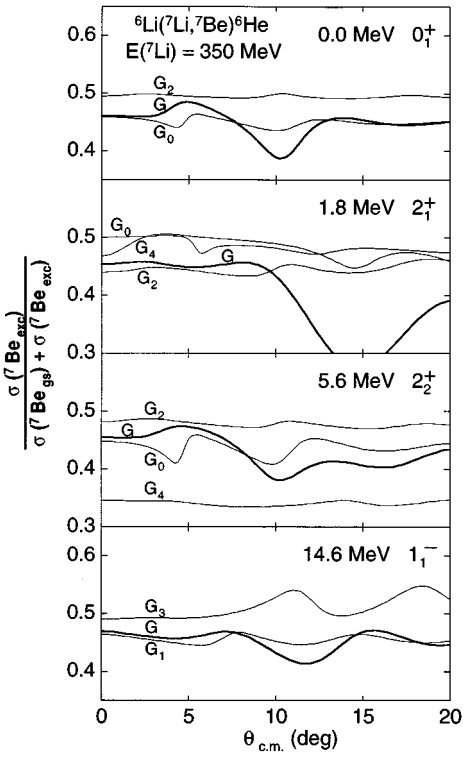

FIG. 7. Calculated cross section ratios $G \equiv \sigma(^7\mathrm{Be_{exc}}) / [\sigma(^7\mathrm{Be_{g.s.}}) + \sigma(^7\mathrm{Be_{exc}})]$ as defined in Eq. (3) for transitions to states in ^{6}He as function of $\theta_{\rm c.m.}$. Also shown are the cross section ratios G_L calculated separately for each contributing value of L (see Sec. IV D). The experimental ratios $G \equiv \sigma(\mathrm{CO}) / \sigma(\mathrm{SNGL})$ averaged over $\theta_{\rm c.m.} = 0°-13°$ are included in Table VII.

V. DISCUSSION

A. States in ^{6}He at $E_x = 0.0$ MeV and $E_x = 1.8$ MeV

The agreement between the experimental and calculated angular distributions as shown in Figs. 3 and 4 is quite good with $\chi^2/F = 3.7$ and 1.2, respectively. In particular, the forward peak for the 0^+ ground state is well described while the data do not show the weak mimimum predicted at $\sim 11°$ which is responsibile for the slightly increased χ^2/F.

A slightly better value χ^2/F for the 0^+ state can be obtained by independently adjusting the contributions for each L value. This leads to higher relative contributions from $L = 4$. However, as mentioned in Sec. IV C, it was felt that a better justified procedure would be based on the incoherent superposition of the central and the tensor interactions with individually adjusted factors. Interestingly, the result for the transition to the most relevant 0^+ ground state leads to essentially equal factors (see Table III). This suggests that the contributions are correctly described by M3Y with a coherent superposition of the central and tensor contributions.

Figures 3 and 4 display the decomposition of the contributions with labels (L, J_p, J_t) resulting from the central and tensor interaction. The majority of contributions belong to only one class each, i.e., either central or tensor. As already pointed out by Anantaraman *et al.* [23] for the much simpler (^{12}C, ^{12}B) and (^{12}C, ^{12}N) reactions on $J^\pi = 0^+$ targets, the noncentral character of the tensor force can lead to cross terms between L_p and L_t ($\vec{J_p} = \vec{L_p} + \vec{S_p}$, $\vec{J_t} = \vec{L_t} + \vec{S_t}$) which makes the identification of Gamow-Teller components more difficult than in (p,n) or (n,p) charge-exchange reactions where $L_p = 2$ is excluded. The situation for the (^{7}Li, ^{7}Be) reaction is even more complex because of the presence of four values for J_p, namely, $J_p = 0$, 1, 2, and 3, and not only $J_p = 0$ and 1 as assumed in Eqs. (1) and (2). Nevertheless, for both states the experimental cross section ratios G of Table I for small angles are close to the value expected for $\Delta S = 1$ transitions as given by Eq. (5) (see also Sec. V E).

Whereas the transition to the 0^+ ground state carries significant B(GT) strength as supported by the strong (0,1,1) cross section components near 0°, the B(GT) strength calculated for the 2^+ state is very small. Here, the (0,1,1) cross section component of the central interaction contributes only $\sim 10\%$ to the total cross section near 0°, and the 0° cross section is clearly not proportional to B(GT). Instead, several $L = 2$ transitions dominate for small angles up to 7°, namely, (2,1,3), (2,1,2), and (2,1,1). Interestingly, the transition with $J_t = 3$ is the most dominant one.

The cross sections at angles $\theta > 13°$ are almost exclusively due to $L = 4$ and $L = 6$ transfers. These contributions, namely, (4,1,3) and (6,3,3), are the result of contributions from the tensor interaction which therefore determine the slope of the measured angular distributions at larger angles.

It should be noted that the small value of $\chi^2/F \approx 1.2$ for the 2^+ state is in part due to the small cross sections with consequently large uncertainties at large angles. Improved agreement of the calculated distribution with the data could again empirically be achieved by increasing the contribution

TABLE VII. Calculated cross section ratios $G \equiv \sigma(^7\mathrm{Be}_{\mathrm{exc}}) / [\sigma(^7\mathrm{Be}_{\mathrm{g.s.}}) + \sigma(^7\mathrm{Be}_{\mathrm{exc}})]$ at $\theta = 0°$ for all permitted angular momentum couplings (L, J_p, J_t) of the transitions to the 0^+, 2^+, 2^+, and 1^- states in ^{6}He at $E_x = 0.0$, 1.8, 5.6, and 14.6 MeV, respectively. The quantities G_L and G are the weighted means.

$J_i^\pi \rightarrow J_f^\pi$	E_x (MeV)	L	J_p	J_t	G_i	G_L	G	$J_i^\pi \rightarrow J_f^\pi$	E_x (MeV)	L	Jp	J_t	G_i	G
$1^{1+} \rightarrow 0^+$	0.0	0	1	1	0.46	0.46	0.46							
		2	1	1	0.52	0.50				2	1	2	0.45	
		2	2	1	1.00					2	1	3	0.45	
	2	3	1	0.00						2	2	1	1.00	
	4	3	1	0.00	0.00					2	2	2	0.94	
$1^+ \rightarrow 2^+$	1.8	0	1	1	0.50	0.50	0.45			2	2	3	1.00	
		0	2	2	0.99					2	3	1	0.00	
		0	3	3	0.00					2	3	2	0.00	
		2	0	2	0.00	0.44				2	3	3	0.00	
		2	1	1	0.46					4	1	3	0.51	0.35
		2	1	2	0.45					4	2	2	0.88	
		2	1	3	0.45					4	2	3	1.00	
		2	2	1	1.00					4	3	1	0.00	
		2	2	2	0.96					4	3	2	0.00	
		2	2	3	1.00					4	3	3	0.00	
		2	3	1	0.00					6	3	3	0.00	0.00
		2	3	2	0.00			$1^+ \rightarrow 1^-$	14.6	1	0	1	0.00	0.46
		2	3	3	0.00					1	1	0	0.48	
		4	1	3	0.51	0.47				1	1	1	0.46	
		4	2	2	0.96					1	1	2	0.45	
		4	2	3	1.00					1	2	1	0.99	
		4	3	1	0.00					1	2	2	1.00	
		4	3	2	0.00					1	3	2	0.00	
		4	3	3	0.00					3	1	2	0.51	0.49
		6	3	3	0.00	0.00				3	2	1	0.92	
$1^+ \rightarrow 2^+$	5.6	0	1	1	0.49	0.45	0.46			3	2	2	1.00	
		0	2	2	0.98					3	3	0	0.00	
		0	3	3	0.00					3	3	1	0.00	
		2	0	2	0.00	0.48				3	3	2	0.00	
			2	1	1	0.50				5	3	2	0.00	0.00

with the highest $L = 6$ or by using an incoherent superposition of central and tensor contributions.

The normalization factors of Table VI for the two shell-model states are $f = 0.65$ and $f = 0.71$, respectively. As mentioned previously (see Sec. IV A and Table II), these values include the renormalization due to the experimental and calculated B(GT) values for the transitions to $^7\mathrm{Be}_{\mathrm{g.s.}}$ and $^7\mathrm{Be}_{\mathrm{exc}}$. A corresponding renormalization (see Table III) for the transition to the 0^+ ground state of ^{6}He leads to the corrected normalization factor $f^{\mathrm{corr}} = 0.73$. Such normalization factors close to unity for the transitions to the two shell-model states agree favorably with similar factors found in the (^{12}C, ^{12}B) reaction at $E = 70A$ MeV on several target nuclei (see Table II in Ref. [23]). The latter require a much smaller number of angular momentum labels (L, J_p, J_t). The above results support the suggestion that the (^{7}Li, ^{7}Be) reaction at $E(^7\mathrm{Li}) = 50A$ MeV proceeds by a direct one-step reaction mechanism. The small departures of the normalization factors from unity are due to uncertainties in the nucleon-nucleon interaction, uncertainties in the optical-model parameters for ^{7}Be which could be due to an isospin dependence in the potential well depth for the mirror nuclei ^{7}Li and ^{7}Be, and uncertainties in the transition amplitudes on account of corrections to the p-shell wave functions and possible core excitations (see Ref. [23]).

B. Resonance in ^{6}He at $E_x \approx 5.6$ MeV

As shown in Fig. 5, the strong transition to the state at $\sim$5.6 MeV is well described by the calculations with $\chi^2/F = 3.6$ assuming $J^\pi = 2^+$. Fits were also performed for other values of J^π as shown in the figure. The agreement with the data for assumed $J^\pi = 1^+$, 0^+, and 1^- is slightly worse as reflected by the increased values of χ^2/F from 5.6 to 8.1 (see Table VI). While the assignment $J^\pi = 2^+$ is favored, $J^\pi = 1^-$ cannot be completely ruled out. The ex-

perimental cross section ratio $G=0.39\pm0.04$ is in support of a spin-flip transition with $\Delta S=1$ for this resonance (see Sec. V E). The normalization factors f are large for all spin assignments and range from 12.6 for $J^\pi = 2^+$ to 50.9 for an assumed $J^\pi = 0^+$.

It was initially thought that the resonance could have $J^\pi = 0^+$ because the slope of the exponential tail at larger angles (see Fig. 2) is close to that of the $J^\pi = 0^+$ ground state. However, it was found that the slope of the tail is not determined by the low-L contributions to the transition amplitudes but instead by the high-L contributions which apparently differ for the two 2^+ states at 1.8 and 5.6 MeV.

The resonance at 5.6 MeV is of particular interest as a possible candidate for a soft giant dipole resonance which is one of the manifestations of neutron-halo nuclei [1–7]. The soft $E1$ mode has been established experimentally (e.g., Ref. [7]) as an enhancement of Coulomb dissociation, but it appears that no resonance contribution has so far been identified (see, however, Ref. [17]). A soft giant dipole resonance was initially predicted theoretically for the nucleus ^{6}He at $E_x = 4$–7 MeV [3] by using the cluster orbital shell model [21]. However, the possible existence of such a resonance at low excitation energy in ^{6}He could not be confirmed in more recent calculations [4,5,18–20]. The theoretical approaches included a complex scaling method combined with a microscopic cluster model [4,5], the asymptotic expansion of exact three-body wave functions [18], and the ''*TV* model'' [19,20] which represents a combination of the cluster orbital shell model [21] and the extended cluster model [22].

As noted above, a soft giant dipole resonance with $J^\pi = 1^-$ cannot be completely ruled out by the measured angular distribution, but it appears to be excluded from the measurement of the cross section ratio G which suggests spin-flip (see Sec. V E). The most likely assignment for the resonance at $\sim$5.6 MeV is $J^\pi = 2^+$. A large normalization factor $f\approx 12.6$ is required to explain the strong cross sections. This presumably reflects upon quadrupole admixtures from unbound states, and the p-shell transition amplitudes constitute only a small fraction of the transition strength. The $J^\pi=2^+$ resonance observed in ^{6}He at $\sim$5.6 MeV may be related to the low-lying quadrupole resonances predicted recently for neutron-skin nuclei [52].

Table III lists the excitation energies for all positive-parity states in ^{6}He calculated in the present work for p-shell single-particle states. Also listed are the excitation energies and widths calculated with the ''*TV* model'' [19,20]. The sequence of the calculated J^π values is identical for the two calculations. As already noted by the authors, the excitation energies for the latter calculations appears slightly low. The possibility of a $(2^+, 1^+)$ mixture of the 5.6-MeV resonance was also considered in the present work, but no significantly improved fit could be obtained (see Table VI).

Since the resonance at $E_x\approx 5.6$ MeV is broad, $\Gamma\approx 10.9$ MeV, it was considered desirable to explore the dependence of the calculations on the radial shape of the wave functions. The objective was to possibly explain the large normalization factor f. In order to simulate this effect, two approaches were taken. In one approach the ground-state binding energy was significantly decreased from $B=1.87$ MeV to $B=0.01$ MeV. In another approach the diffuseness a of the potential well generating the ^{6}He single-particle wave function was significantly increased by factors of 2 and 4. The change in binding energy decreased the calculated B(GT) by only $\sim$20%, whereas the renormalization factor f required to describe the data with the smaller calculated cross sections increased by a similar percentage. The product $B(\mathrm{GT})\times f$ increased by only $\sim$2%; that is, it remained essentially constant. The change in the diffuseness a has a slightly larger effect. Increasing a by factors of 2 and 4 decreased B(GT) by factors of $\sim$0.8 and $\sim$0.5, respectively. The renormalization factors increased by essentially the inverse factors, and the product $B(\mathrm{GT})\times f$ changed very little. It decreased by $\sim$3% and $\sim$6%, respectively. Correcting for the calculated B(GT) values requires the renormalization of the calculated cross sections by the ratio of the (unknown) experimental to the calculated B(GT) values. It is therefore concluded that the large renormalization factor cannot be explained by the shape of weakly bound or diffuse single-particle wave functions.

C. Resonance in ^{6}He at $E_x\approx$ 14.6 MeV

The angular distribution measured for the resonance at 14.6 MeV, Fig. 6, is well described with χ^2/F from 2.4 to 4.7 as a state with $J^\pi = 1^-$ or 2^- (see Table VI). A strong enhancement with normalization factors of $f = 15$–40 presumably reflects upon mixing with unbound states. The cross section ratio $G=0.43\pm0.04$ suggests a spin-flip transition. This is confirmed by several other reactions [8] which interpret this resonance as a spin dipole resonance. The ^{6}Li (π^-,γ) ^{6}He radiative pion capture reaction [12,13] and the ^{6}Li(e^-,π^+) ^{6}He and ^{6}Li(γ,π^+) ^{6}He photopion reactions [16] selectively excite simple $1p$–$1h$ spin-flip states. The resonance was also observed in 60-MeV (n,p) data [11]. A possible splitting of this resonance into two or even three resonances in the range $E_x = 13$–18 MeV has also been reported [14–16].

D. Resonance in ^{6}He at $E_x\approx$ 23.3 MeV

The angular distribution for this resonance shown in Fig. 2 is very flat and displays only a minor increase towards smaller angles. Attempts to fit the distribution assuming a direct reaction mechanism were unsuccessful as seen from Table VI. However, the cross section ratio of $G=0.43\pm0.07$ suggests a spin-flip transition. It is concluded that the measured angular distribution is not compatible with a low-spin direct reaction mechanism. Possible explanations include a high-spin resonance or a complicated structure leading to a compound nucleus reaction mechanism.

E. Spin-flip characteristics

Equations (1) to (5) for the cross section ratios G near $\theta = 0°$ are strictly valid only for the angular momentum labels (L,J_p,J_t) with $J_p = 0$ or 1. Table VII shows that for the transitions to the four final states in ^{6}He all calculated contributions with the labels $(L,1,J_t)$ are indeed in the range $G_i = 0.45$–0.52. This means that the transitions to the ground and excited states of ^{7}Be have about equal cross sections as expected from Eq. (5) for Gamow-Teller transitions with $\Delta S=1$. However, a few contributions $(L,0,J_t)$ with $J_p = 0$ which have $G_i\equiv 0.00$ are also present. Further-

more, contributions $(L,2,J_t)$ and $(L,3,J_t)$ with $J_p = 2$ and 3 are present. All terms with $J_p = 2$ strongly favor the transition to ^{7}Be$_{exc}$ with $G_i \equiv 1$ (for $L+J_p+J_t$ = odd) or at least $G_i > 0.9$ (for $L+J_p+J_t$ = even). All terms with $J_p = 3$ allow only transitions to ^{7}Be$_{g.s.}$; hence, $G_i \equiv 0$. These additional contributions with $J_p = 0$, 2, and 3 influence the averaged experimental cross section ratios G.

Another consideration which may affect the interpretation of the measured cross section ratios G is the presence of the tensor interaction which allows cross terms between L_p and L_t ($\vec{J_p} = \vec{L_p} + \vec{S_p}$, $\vec{J_t} = \vec{L_t} + \vec{S_t}$) which make the identification of Gamow-Teller components more difficult than in (p,n) or (n,p) charge-exchange reactions where $L_p = 2$ is excluded. Even for $J_p = 1$, the orbital angular momentum L_p in the equation $\vec{J_p} = \vec{L_p} + \vec{S_p}$ allows $L_p = 0$, but $L_p = 2$ is also permitted by the tensor interaction. Only for $L_p = 0$ can a clear distinction be made between Fermi ($S_p = 0$) and Gamow-Teller ($S_p = 1$) transitions.

The experimental cross section ratios G listed in Table I suggest that, according to Eq. (5), all observed states and resonances including the resonance at 23.3 MeV are associated with spin-flip Gamow-Teller transitions, that is, $\Delta S = 1$. This is expected for the 0^+ ground state in ^{6}He and the 2^+ state at 1.8 MeV, and it is suggested by other experiments (see Sec. V C) for the resonance at $\sim$14.6 MeV. A value of $G = 0.40 \pm 0.08$ was also observed [31] for the Gamow-Teller transition to the ground state of ^{12}B. It is therefore concluded that the transitions to the resonances at $\sim$5.6 MeV, $\sim$14.6, and 23.3 MeV must also have spin-flip character. The validity of the rules of Nakayama *et al.* [29] results from the fact that the contributions with $J_p = 1$ and labels $(L,1,J_t)$ dominate at small angles as can be seen from Figs. 3–6. This result is in agreement with the averaged calculated ratio $G \approx 0.46$ at $\theta = 0°$ from Table VII which signifies spinflip transitions.

Interestingly, Fig. 4 shows that the most important term at small angles for the transition to the 2^+ state at 1.8 MeV is (2,1,3), and while of spin-flip type with $S_p = 1$ and $S_t = 1$, the total angular momentum is $J_t = 3$ which permits $L_t = 2$ *and* $L_t = 4$. The small contribution from $L = 0$ with the angular momentum label (0,1,1) at small angles demonstrates that 0° cross sections are not proportional to B(GT) except presumably for strong transitions.

The angular dependence of the calculated cross section ratios $G \equiv \sigma(^7\text{Be}_{exc}) / [\sigma(^7\text{Be}_{g.s.}) + \sigma(^7\text{Be}_{exc})]$, which is displayed in Fig. 7, oscillates with angle and shows minima at angles in the range 10°–15°. These minima at 15° for the 2^+ state at 1.8 MeV are most pronounced. The minima occur near the maxima in the calculated angular distributions of the contribution with the highest L values. For $J^\pi = 0^+$, 1^-, and 2^+, the highest L values are $L = 4$, 5, and 6 and belong to the (L,J_p,J_t) labels with $J_p = 3$, namely, (4,3,1), (5,3,2), and (6,3,3). Therefore, there are no contribution for transitions to ^{7}Be$_{exc}$ and $G_i \equiv 0$. One might consider measuring the minima as a signature for these contributions, but this suggestion is not too promising because of the small cross sections at large angles.

VI. SUMMARY AND CONCLUSIONS

Transitions to the known 0^+ and 2^+ states in ^{6}He at $E_x = 0.0$ and 1.8 MeV (weak) and three strong and broad resonances at $E_x \approx 5.6$, 14.6, and 23.3 MeV have been observed with the ^{6}Li(^{7}Li,^{7}Be)^{6}He charge-exchange reaction at $E(^7\text{Li}) = 350$ MeV. The reaction is well suited to identify high-lying resonances. Angular distributions have been measured for all states, and coincidences with 430-keV Doppler-shifted γ rays from the deexcitation of the first-excited state in ^{7}Be$_{exc}$ were recorded.

The reaction mechanism for the ^{6}Li(^{7}Li,^{7}Be)^{6}He charge-exchange reaction at $E(^7\text{Li}) = 50A$ MeV can be understood in terms of a direct one-step reaction mechanism. The structureless angular distributions are well described by microscopic finite-range distorted-wave calculations with theoretical shell-model transition amplitudes and a nucleon-nucleon interaction which includes central and tensor components. The internal structures of the projectile and the ejectile make it necessary to introduce angular momentum labels (L,J_p,J_t) where L is the orbital angular momentum transfer in the relative coordinates, and J_p and J_t are, respectively, the total angular momenta transferred to the projectile and the target. Since J_p can take on four different values, the number of possible angular momentum labels can be quite large, particularly for transitions between targets and residual states with $J^\pi \neq 0$. The transitions to the two shell-model states with $J^\pi = 0^+$ and 2^+ are quantitatively described. The strong and broad resonances at $\sim$5.6 MeV and $\sim$14.6 MeV are interpreted as 2^+ and $(1,2)^-$ resonances, respectively, with enhancements presumably from admixtures of unbound states. It appears that the resonance at $\sim$5.6 MeV is not a soft giant dipole resonance. The strong resonance at $\sim$23.2 MeV cannot be explained with a low-L direct reaction mechanism.

While the quantitative description, especially of the shell-model states with *known* transition amplitudes, is quite satisfactory, it is also clear that the measured structureless angular distributions alone provide only limited information about the internal structures or the values of J^π of the final states unless a strong 0° peak suggests an angular momentum transfer of $L = 0$. Cross sections measured at 0° are not necessarily proportional to B(GT). The exponential tails are due to the superposition of high-L angular components which are usually the result of the couplings between high J_p and J_t values due to the tensor interaction. The interpretation of angular distribution from the (^{7}Li,^{7}Be) reaction is more complicated than for the (n,p) reaction and certain other heavy-ion charge-exchange reactions.

The cross section ratios $G \equiv \sigma(^7\text{Be}_{exc}) / [\sigma(^7\text{Be}_{g.s.}) + \sigma(^7\text{Be}_{exc})]$ obtained from the coincidence measurements with 430-keV γ rays were found in the range 0.36–0.46, suggesting spin-flip transitions. This conclusion is probably correct because of the calculated dominance of $J_p = 1$ angular momentum transfer to the projectile. The general application of the rules of Nakayama *et al.* [29] represented by Eqs. (1)–(5) must be considered with some caution, though, because of the often large number of contributions with angular momentum labels (L,J_p,J_t) and $J_p = 0$, 1, 2, and 3. The rules are expected to be valid if contributions with $J_p = 0$ or 1 dominate at small angles and if interference from the tensor interaction can be neglected.

ACKNOWLEDGMENTS

The authors acknowledge the support provided by the technical staff of the National Superconducting Cyclotron

Laboratory, helpful discussions with N. Anantaraman, F. D. Becchetti, K. T. Hecht, A. Nadasen, and R. Ronningen, and the important help with computer analysis by M. Young (REU summer student 1995). The research was supported in part by the National Science Foundation Grants Nos. PHY-9208468 (UM, Ann Arbor) and PHY-92-14992 (NSCL).

[1] P. G. Hansen and B. Jonson, Europhys. Lett. **4**, 409 (1987).
[2] I. Tanihata *et al.*, Phys. Rev. Lett. **55**, 2676 (1985); Phys. Lett. **160B**, 380 (1985); Nucl. Phys. **A488**, 113 (1988); **A553**, 361c (1993).
[3] Y. Suzuki, Nucl. Phys. **A528**, 395 (1991).
[4] A. Csótó, Phys. Rev. C **48**, 165 (1993).
[5] A. Csótó, Phys. Rev. C **49**, 2244 (1994).
[6] P. G. Hansen, A. S. Jensen, and B. Jonson, Annu. Rev. Nucl. Part. Sci. **45**, 591 (1995).
[7] I. Tanihata, Prog. Part. Nucl. Phys. **35**, 505 (1995); J. Phys. G **22**, 157 (1996).
[8] F. Ajzenberg-Selove, Nucl. Phys. **A490**, 1 (1988).
[9] K. P. Jackson, A. Celler, W. P. Alford, K. Raywood, R. Abegg, R. E. Azuma, C. K. Campbell, S. El-Kateb, D. Frekers, P. W. Green, O. Häusser, R. L. Helmer, R. S. Henderson, K. H. Hicks, R. Jeppesen, P. Lewis, C. A. Miller, A. Moalem, M. A. Moinester, R. B. Schubank, G. G. Shute, B. M. Spicer, M. C. Vetterli, A. I. Yavin, and S. Yen, Phys. Lett. B **201**, 25 (1988).
[10] D. S. Sorenson, X. Aslamoglou, F. P. Brady, J. R. Drummond, R. C. Haight, C. R. Howell, N. S. P. King, A. Ling, P. W. Lisowski, B. K. Park, J. Rapaport, J. L. Romeo, W. Tornow, and J. L. Ullmann, Phys. Rev. C **45**, R500 (1992).
[11] F. Brady, G. A. Needham, J. L. Romero, C. M. Castaneda, T. D. Ford, J. L. Ullmann, and M. L. Webb, Phys. Rev. Lett. **51**, 1320 (1983); F. Brady, G. A. Needham, J. L. Ullmann, C. M. Castaneda, T. D. Ford, N. S. P. King, J. L. Romero, M. L. Webb, V. R. Brown, and C. H. Poppe, J. Phys. G **10**, 363 (1984).
[12] H. W. Baer, J. A. Bistirlich, K. M. Crowe, N. de Botton, J. A. Helland, and P. Truöl, Phys. Rev. C **8**, 2029 (1973).
[13] J. P. Perroad, A. Perrenoud, J. C. Alder, B, Gabioud, C. Joseph, J. F. Loude, N. Morel, M. T. Tran, E. Winkelmann, H. von Fellenberg, G. Strassner, P. Truöl, W. Dahmke, H. Panke, and D. Renker, Nucl. Phys. **A453**, 542 (1986).
[14] J. C. Roynette, M. Arditi, J. C. Jacmart, F. Mazloum, M. Riou, and C. Ruhla, Nucl. Phys. **A95**, 545 (1967).
[15] F. P. Brady, Phys. Rev. C **16**, 31 (1977).
[16] K. Shoda, M. Torikoshi, O. Sasaki, S. Toyama, T. Kobayashi, A. Kagaya, and H. Tsubota, Phys. Rev. C **33**, 2179 (1986).
[17] S. B. Sakuta, A. A. Ogloblin, O. Ya. Osadchy, Yu. A. Glukhov, S. N. Ershov, and F. A. Gareev, Europhys. Lett. **28**, 111 (1994).
[18] B. V. Danilin, M. V. Zhukov, J. S. Vaagen, and J. M. Bang, Phys. Lett. B **302**, 129 (1993).
[19] S. Aoyama, S. Mukai, K. Kato, and K. Ikeda, Prog. Theor. Phys. **93**, 99 (1995).
[20] S. Aoyama, S. Mukai, K. Kato, and K. Ikeda, Prog. Theor. Phys. **94**, 343 (1995); K. Kato, S. Aoyama, S. Mukai, and K. Ikeda, Nucl. Phys. **A588**, 29c (1995).
[21] Y. Suzuki and K. Ikeda, Phys. Rev. C **38**, 410 (1988).
[22] K. Ikeda, Nucl. Phys. **A538**, 355c (1992).
[23] N. Anantaraman, J. S. Winfield, S. M. Austin, J. A. Carr, C. Djalali, A. Gillibert, W. Mittig, J. A. Nolen, and Zhan Wen Long, Phys. Rev. C **44**, 398 (1991).
[24] F. Osterfeld, N. Anantaraman, S. M. Austin, J. A. Carr, and J. S. Winfield, Phys. Rev. C **45**, 2854 (1992).
[25] S. M. Austin, Nucl. Phys. **A577**, 51c (1994).
[26] M. E. William-Norton, F. Petrovich, K. W. Kemper, G. M. Hudson, R. J. Puigh, and A. F. Zeller, Nucl. Phys. **A275**, 509 (1977).
[27] J. Cook, K. W. Kemper, P. V. Drumm, L. K. Fifield, M. A. C. Hotchkis, T. R. Ophel, and C. L. Woods, Phys. Rev. C **30**, 1538 (1984).
[28] S. Nakayama, T. Yamagata, K. Yuasa, M. Tanaka, M. Inoue, T. Itahashi, and H. Ogata, Phys. Lett. B **195**, 316 (1987); **246**, 342 (1990).
[29] S. Nakayama, T.Yamagata, M. Tanaka, M. Inoue, K. Yuasa, T. Itahashi, H. Ogata, N. Koori, and K. Shima, Nucl. Instrum. Methods A **302**, 472 (1991); Phys. Rev. Lett. **67**, 1082 (1991).
[30] W. T. Chou, E. K. Warburton, and B. A. Brown, Phys. Rev. C **47**, 163 (1993).
[31] T. Annakkage *et al.* (unpublished); Ph.D. thesis, University of Michigan, 1995; J. Jänecke, T. Annakkage, K. Pham, D. A. Roberts, J. A. Brown, G. Crawley, S. Danczyk, D. J. Mercer, J. Stasko, G. J. S. Winfield, G. H. Yoo, G. P. A. Berg, and M. Fujiwara, Nucl. Phys. **A599**, 191c (1996).
[32] O. Häusser, M. A. Lone, T. K. Alexander, S. A. Kushneriuk, and J. Gascon, Nucl. Instrum. Methods **213**, 301 (1983).
[33] T. Annakkage, J. Jänecke, K. Pham, D. A. Roberts, G. P. A. Berg, and J. S. Winfield, Nucl. Instrum. Methods A **353**, 24 (1994).
[34] A. Erell, J. Alster, J. Lichtenstadt, M. A. Moinester, J. D. Bowman, M. D. Cooper, F. Irom, H. S. Matis, E. Piasetzki, and U. Sennhauser, Phys. Rev. C **34**, 1822 (1986); A. Erell, Ph.D. thesis, Tel-Aviv University, 1984.
[35] F. Irom, J. D. Bowman, G. O. Bolme, E. Piastzky, U. Sennhauser, J. Alster, J. Lichtenstadt, M. Moinester, J. N. Knudson, S. H. Rokni, and E. R. Siciliano, Phys. Rev. C **34**, 2231 (1986).
[36] J. Jänecke, K. Pham, D. A. Roberts, D. Stewart, M. N. Harakeh, G. P. A. Berg, C. C. Foster, J. E. Lisantti, R. Sawafta, E. J. Stephenson, A. M. van der Berg, S. Y. van der Werf, S. E. Muraviev, and M. H. Urin, Phys. Rev. C **48**, 2828 (1993).
[37] K. Pham, J. Jänecke, D. A. Roberts, M. N. Harakeh, G. P. A. Berg, S. Chang, J. Liu, E. J. Stephenson, B. F. Davis, H. Akimune, and M. Fujiwara, Phys. Rev. C **51**, 526 (1995).
[38] S. Cohen and D. Kurath, Nucl. Phys. **73**, 1 (1965).
[39] J. Stevenson, B. A. Brown, Y. Chen, J. Clayton, E. Kashy, D. Mikolas, J. Nolen, M. Samuel, B. Sherrill, J. S. Winfield, Z. Q. Xie, R. E. Julies, and W. A. Richter, Phys. Rev. C **37**, 2220 (1988).
[40] R. E. Julies, W. A. Richter, and B. A. Brown, S. Af. J. Phys. **15**, 35 (1992).
[41] A. N. Ostrowski *et al.*, Phys. Lett. B **338**, 13 (1994).

[42] B. A. Brown, A. Etchegoyen, and W. D. M. Rae, computer code OXBASH, The Oxford-Buenos-Aires-MSU Shell-Model Code, MSUCL Report No. 524, 1988 (unpublished).
[43] D. J. Millener and D. Kurath, Nucl. Phys. **A255**, 315 (1975).
[44] P. M. Preedom and B. H. Wildenthal, Phys. Rev. C **6**, 1633 (1972).
[45] J. Cook and J. A. Carr, computer code FOLD, Florida State University, 1988 (unpublished).
[46] F. Petrovich and D. Stanley, Nucl. Phys. **A275**, 487 (1977).
[47] W. G. Love and M. A. Franey, Phys. Rev. C **24**, 1073 (1981).
[48] M. A. Franey and W. G. Love, Phys. Rev. C **31**, 488 (1985).
[49] F. Petrovich, R. J. Philpott, A. W. Carpenter, and J. A. Carr, Nucl. Phys. **A425**, 609 (1984).
[50] A. Nadasen, J. Brusoe, J. Farhat, T. Stevens, J. Williams, L. Nieman, J. S. Winfield, R. E. Warner, F. D. Becchetti, J. Jänecke, T. Annakkage, and H. S. Govinden, Phys. Rev. C **52**, 1884 (1995).
[51] A. Nadasen, M. McMaster, M. Fingal, J. Tavormina, P. Schwandt, J. S. Winfield, M. F. Mohar, F. D. Becchetti, J. W. Jänecke, and R. E. Warner, Phys. Rev. C **39**, 536 (1989).
[52] M. Yokoyama, T. Otsuga, and N. Fukunishi, Phys. Rev. C **52**, 1122 (1995).